Check for updates

Interplay of piezoresponse and magnetic behavior in Bi$_{0.9}$A$_{0.1}$FeO$_{2.95}$ (A = Ba, Ca) and Bi$_{0.9}$Ba$_{0.05}$Ca$_{0.05}$FeO$_{2.95}$ co-doped ceramics

G. Mangamma, [ID] [a] B. K. Das,[a] B. Ramachandran,[b] M. S. Ramachandra Rao[b] and T. N. Sairam [ID] *[a]

Extensive piezoresponse force microscopy (PFM) and magnetic force microscopy (MFM) measurements in conjunction with piezoresponse spectroscopy have been carried out on pellets of Bi$_{0.9}$A$_{0.1}$FeO$_{2.95}$ (A = Ba, Ca) and Bi$_{0.9}$Ba$_{0.05}$Ca$_{0.05}$FeO$_{2.95}$ co-doped ceramic samples in order to characterize their ferroelectric and magnetic nature and correlate the findings with our recent far-infrared spectroscopic studies on these samples. We are able to clearly discern the switching behavior of the 71° and 109° ferroelectric domains as distinct from that of the 180° domains in both pristine and Ba-doped bismuth ferrite samples. While substitution of Ba at the Bi site in bismuth ferrite does not affect the ferroelectric and magnetic properties to a great extent, Ca-doped samples show a decrease in their d_{33} values with a concomitant increase in their magnetic behavior. These results are in agreement with the findings from our far-infrared studies.

1 Introduction

BiFeO$_3$ is a room temperature multiferroic that has a rhombohedrally distorted perovskite structure with the *R3c* space group. It undergoes a transition from the paraelectric to ferroelectric phase at a Curie temperature of 1100 K,[1] accompanied by the onset of the polarization along the $\langle 111 \rangle_{pc}$ pseudo cubic (pc) direction because of the stereochemical activity of the lone-pair electrons over Bi^{3+} ions leading to polar atomic displacements along that direction and anti-phase tilting of the adjacent FeO$_6$ octahedra.[2,3] Increased interest in the ferroelectric property of this material is due to the high value of spontaneous polarization (P_s) ($\sim$90 μC cm^{-2}) predicted through *ab initio* calculations.[3,4] Experimentally observed values of P_s are $\sim$ 40 μC cm^{-2} in bulk ceramic form[5] and about 90−150 μC cm^{-2} in thin film form.[6,7] The magnetic structure of this compound is replete with a host of magnetic interactions:[2,8] it exhibits G-type anti-ferromagnetism and a spiral spin arrangement with Néel temperature T_N = 647 K. This antiferromagnetic spin structure itself arises from a superexchange (SE) interaction between the neighboring spins of Fe ions mediated *via* oxygen atoms. In addition, antisymmetric exchange between the neighboring spins gives rise to Dzyaloshinskii–Moriya (DM) interaction, while an interaction between the crystal field and the orbital

magnetic moment results in single ion anisotropy (SIA). Competition between the DM and superexchange interactions leads to a canted spin structure.[9] In the case of BiFeO$_3$, these canted spin structure forms an array in a regular fashion over a distance of 62 nm along the $\langle 10\bar{1} \rangle_{pc}$ direction, which is known as spin cycloid. The average magnetic moment over the spin cycloid is found to be zero as each spin has its mirror image in the cycloidal spin arrangement (see Fig. 6). Therefore, the macroscopic magnetization of BiFeO$_3$ gets hampered by cycloidal spin arrangement.

It is desirable to achieve suppression of the spin-cycloid in BiFeO$_3$ at room temperature to pave way for enhanced magnetic properties. This can be realized through chemical substitution,[10–17] inducing strain in thin films,[18–21] high magnetic fields,[22–27] hydrostatic pressure[28–30] and finite size effects.[31–36] Of these, aliovalent doping controls the chemistry of the material and often could result in increased chemical pressure that would work similar to applying hydrostatic pressure externally. To this end, we have synthesized Ba-, Ca- and Ba/Ca co-doped samples. Our recent infrared reflectance and low frequency Raman studies[37] on these Ba, Ca and Ba–Ca co-doped samples to monitor the behavior of their spin wave excitation (SWE) spectra, revealed that Ca-doped BiFeO$_3$ sample showed a near-complete suppression of the SWEs. From our recent magnetic studies, the ceramic BiFeO$_3$ sample was found to develop weak ferromagnetic order at low-temperature.[38,39] This improvement in the magnetic property was understood through the destruction of the cycloidal spin structure driven by an increase in single ion anisotropy and anharmonicity of the spin cycloid,[40] as was evidenced from the direct observation of a partial

[a]Materials Science Group, Indira Gandhi Centre for Atomic Research & Homi Bhabha National Institute, Kalpakkam, Tamil Nadu, 603102, India

[b]Department of Physics, Nano Functional Materials Technology and MSRC, Indian Institute of Technology Madras, Chennai, 600036, Tamil Nadu, India. E-mail: sairamtn@gmail.com

suppression of the spin wave excitations from our far-infrared reflectance measurements at low temperature.[41] A similar mechanism could be at play in the doped $BiFeO_3$ system as well. In order to gain a better understanding, we have, in this work, directly studied the ferroelectric and magnetic properties of these doped samples through piezoresponse force microscopy (PFM) and magnetic force microscopy (MFM). Using the phase and 'mag' (short for magnitude) images from the PFM data, it is found that Ba-doped sample retains ferroelectricity, while the Ca-doped sample shows weakened ferroelectric properties. In contrast, MFM studies revealed enhanced magnetism for the Ca doped sample as compared to the pristine sample. These results corroborate the conclusions from our IR studies. In addition, the studies on $Bi_{0.9}A_{0.1}FeO_{2.95}$ (A = Ba, Ca) revealed that Ca and the Ba/Ca co-doped sample show improved magnetic and magnetoelectric properties.[42,43] This is also evident through the near-complete suppression of spin wave excitations observed in our far-infrared data on Ca-doped and co-doped samples brought about by the destruction of the spin cycloid *via* doping.[37]

Here, we present the results of extensive piezoelectric force microscopy (PFM) and magnetic force microscopy (MFM) studies that we carried out on $Bi_{0.9}A_{0.1}FeO_{2.95}$ (A = Ba, Ca). All the samples were found to have piezoelectric response. We have acquired mag and phase images for all the samples. The obtained symmetric loops (phase and mag) due to switching of electric polarization suggest the ferroelectric behavior of the sample. From MFM measurements, the Ca-doped $BiFeO_3$ sample among all is found to have improved magnetic properties as compared to its pristine counterpart.

2 Experimental

On doping with Ca and Ba in $BiFeO_3$, a structural transition from rhombohedral to orthorhombic crystal structure is seen for the dopant concentration, $x \geq 0.1$.[44] Hence, a dopant concentration of 10% is chosen for our studies in order to retain the rhombohedral phase, as in pristine $BiFeO_3$. Ceramic samples of $BiFeO_3$ (BFO), $Bi_{0.9}Ba_{0.1}FeO_{2.95}$ (BBFO), $Bi_{0.9}Ba_{0.05}Ca_{0.05}FeO_{2.95}$ (BBCFO) and $Bi_{0.9}Ca_{0.1}FeO_{2.95}$ (BCFO) were synthesized through modified sol–gel method. Citric acid ($C_6H_8O_7$), taken in a molar ratio of 1 : 1 with metal nitrates, was first dissolved in a solvent of 100 ml distilled water and ethanol. Iron nitrate and bismuth nitrate with a molar ratio of 1 : 1.05 were dissolved in the above solution and thoroughly mixed following which 5 ml of nitric acid and 5 ml of hydrogen peroxide were added to the solution with constant stirring. Then the solution was refluxed for 2 hours at 90 °C to form a gel, which was dried at 300 °C for 1 hour to get bismuth ferrite precursor in powder form. The obtained powder was calcined at 600 °C for one hour and the sintered at 850 °C to get the desired phase pure sample as confirmed from X-ray diffraction (XRD) measurements. Phase purity of the samples was confirmed through powder X-ray diffraction.[44] These samples were pelletized into disc form having a radius of 10 mm and thickness of 1 to 2 mm. These pellets were then sintered at 850 °C for 6 hours. The density of the sintered pellet was found to be greater than

90% of the theoretical density. After this, these pellets were polished to mirror finish using diamond paste and then cleaned with acetone. Post polishing, the pellets were heated at 400 °C for 4 hours in order to remove any surface residual stress that may have been generated due to the mechanical polishing process. The high quality of the samples were also established from the infrared reflectance spectra of these samples,[37,39] wherein we could observe all the allowed phonon modes ($4A_1 + 9E$) corresponding to the rhombohedral phase, with no trace of any impurity phase. From Rietveld refinement of the X-ray diffraction patterns of these samples, a reduction of unit cell volume is observed in all the doped samples compared to the pristine sample.[44] To mention specifically in terms of changes in local structure, Fe–O1 and Fe–O2 bond lengths as well as Fe1–O–Fe2 bond angle are all found to decrease in the case of the doped samples.[37] The $\Delta V/V$ values of the doped samples with respect to the pristine sample are as follows: BBFO: -1.22%; BBCFO: -1.23% and BCFO: -2.08%. Thus, the BCFO sample is found to have the least unit cell volume, Fe–O bond lengths and bond angle. Moreover, the different types of magnetic interactions present in bismuth ferrite are expected to get influenced by this doping-induced increase in chemical pressure. Piezoresponse force microscopy (PFM) images of pristine and doped BFO samples were acquired using a scanning probe microscope (SPM) (NT-MDT, NTEGRA, Russia). An electrically conductive tip (A diamond-like carbon coated stiff cantilever ($100 \times 35 \times 2$ μm) having a stiffness constant $k = 12$ N m^{-1} with resonance frequency = 250 kHz) is employed. An ac bias voltage was used for measuring the piezoelectric response in the contact mode in PFM measurements. The amplitude (also called 'mag') of the cantilever deflection is directly proportional to the strength of the piezoresponse. The 'phase' part of the signal represents the orientation of the piezoelectric domains.[45,46] Piezoresponse spectroscopy experiments were carried out in a voltage range of +20 to −20 V to see the ferroelectric switching behavior of each sample.

MFM studies were carried out using a silicon probe, whose tip is coated with magnetic cobalt chromium (CoCr). The tip having a radius of 25–35 nm and resonant frequency of 40 kHz has a nominal coercivity of 0.04 T, magnetic moment of 10^{-13} emu and stiffness constant of 2.8 N m^{-1}. The tip detects the magnetic interactions between the tip and the sample, which are then used to image the spatial distribution of magnetic fields and thus reconstruct the magnetic structure of the sample. During the measurement, the MFM tip is well lifted off from the sample surface in such a way that the magnetic forces (long range) and the atomic forces (short range) between the tip and sample surface can be distinguished from each other. MFM operates in this non contact mode, where the resonance frequency of the tip is in the range of 10–100 kHz. MFM maps the phase and the resonant frequency during the scanning of sample surface at a constant height. A repulsive magnetic force between the tip and sample surface shifts the resonance frequency to higher value and there is an increase in the phase shift resulting in brighter contrast, while an attractive magnetic force shifts the resonance curve to lower frequency and there is a decrease in the phase shift resulting in dark contrast. Here,

MFM studies were carried out in dual pass mode. In the first pass, the tip is in contact mode to elucidate topography, whereas in the second pass the tip is kept at a constant height and follows the contours of the topography line to map the phase.[47]

3 Results and discussion

3.1 Pristine BiFeO₃ ceramic pellet

3.1.1 PFM study. The ferroelectric properties of $BiFeO_3$ sample has been investigated through piezoresponse force microscopy measurements. Fig. 1 displays the topography, mag and phase images of pristine BFO ceramic sample (scan area~$15 \times 15 \mu m^2$) obtained at a few selected dc voltages *i.e.*, 0, 1, 5, 10, 0, −1, −5, −10 and 0 V (the voltages are selected to complete the hysteresis cyclic order). In the PFM phase image of the $BiFeO_3$, the Piezo-domains, which get polarized in perpendicularly upward and downward directions, are shown by bright and dark contrasts, respectively. Dark and bright regions seen in mag image represent the strength of piezoelectricity. Well defined piezoelectric domains are clearly observed in mag and phase images (see Fig. 1) at $V_{dc} = 0$ V. Similarly, different orientations of various domains are observed as contrast in phase images. The evolution of these domains have been followed as a function of dc voltage. While, we did not observe any significant changes in surface morphology, dramatic changes were seen in the mag and phase images. We were able to locate a number of piezoelectric domains ranging from micron to nanometer size (see the highlighted portion of the mag and phase images by the loops with respect to applied voltage in Fig. 1), which showed significant changes with applied dc voltage. First, let us consider the variation in V_{dc} from 1 to 10 V. For $V_{dc} = 1$ V, all of these ferroelectric domains show no change, whereas there is a noticeable change seen in both phase and mag images for $V_{dc} = 5$ V. Notice that the two domains highlighted (Fig. 1) by the yellow colored loops in phase and mag images at 5 V become brighter and darker, respectively, while they don't show further change at 10 V. The other two domains highlighted with white colored loops are noticed to have significant changes at 10 V (the domains seen in phase and mag images become correspondingly brighter and darker, respectively).

Further, the evolution of the piezoelectric domains have been followed with respect to applied negative dc voltage, where we could find correlated changes. Thus, the domains highlighted by yellow loops undergo switching at an applied dc voltage of 5 V, whereas the domains highlighted by white loops undergo switching at an applied dc voltage of 10 V. Correlations observed in PFM images are described further in relation to different possible switching angles. In the rhombohedral $BiFeO_3$, there are three possible switching of ferroelectric domains, which are at an angle $71°$, $109°$ and $180°$ with the polarization direction along $\langle 111 \rangle_{pc}$ pseudo cubic direction[48,49] as shown in Fig. 2. As our sample is polycrystalline, the ferroelectric domains are randomly oriented. The underlying principle and the phenomenon of switching a ferroelectric domain in $BiFeO_3$ through applying electrical energy are as follows.[48]
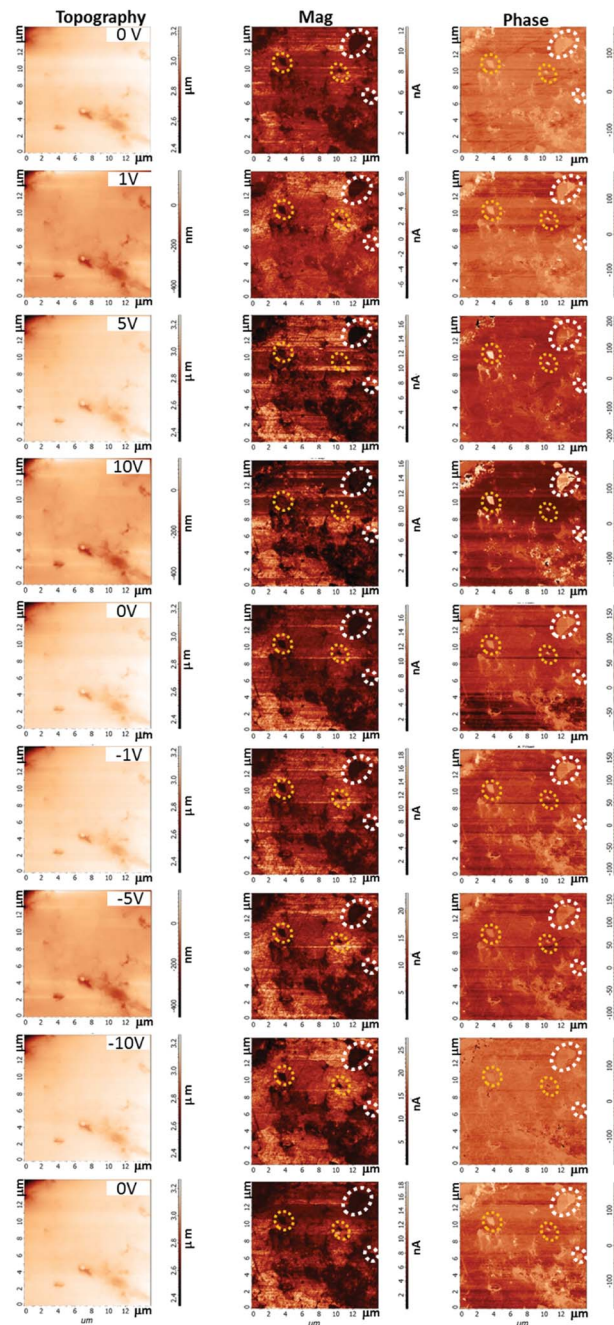

Fig. 1 Topography, mag and phase images of BFO sample at a few selected dc voltages. The yellow and white dotted loops are the regions of magnetic domains which show noticeable changes with applied dc voltage.

1. The applied electrical energy needs to overcome the energy barrier associated with polarization and stress energy of the ferroelectric domain and its surrounding domains.

2. Larger the applied electric field, larger is the switching angle *i.e.*, the domain with larger switching angle requires ample amount of electrical energy for switching as the polarization vector undergoes a larger rotation. Whereas the smaller switching angle domain needs lesser amount of electrical energy as the polarization vector rotates through a smaller
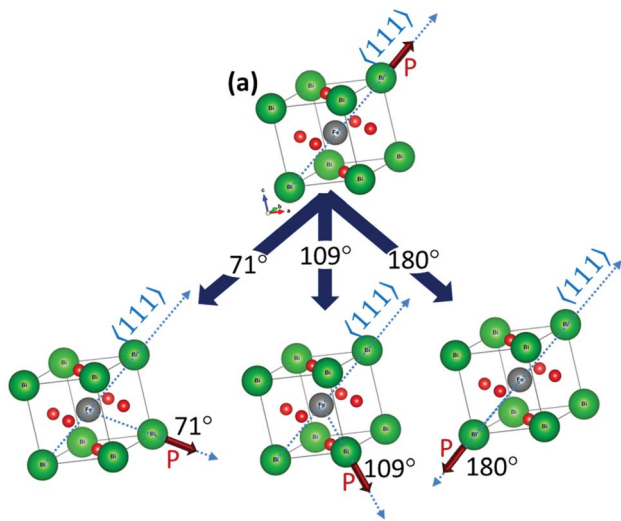
Fig. 2 Schematic of 71°, 109° and 180° domain switching in rhombohedral BiFeO₃.
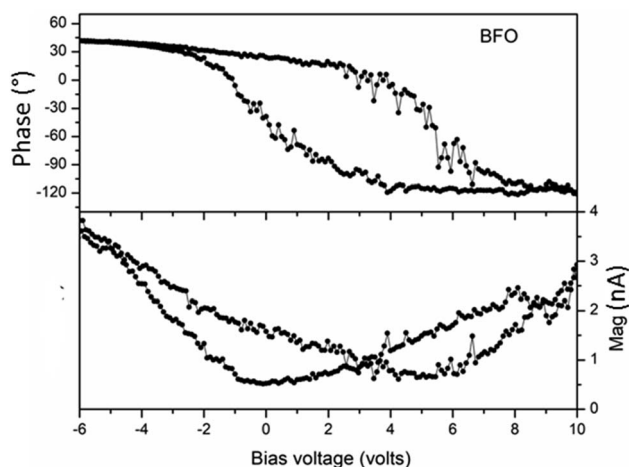

Fig. 3 Phase and mag loops of pristine BFO sample.

angle. Therefore, as we go from 71°–109°–180°-ferroelectric domains, the applied electrical energy needed for switching also increases accordingly.

3. The stress energy associated with a switched domain depends on switching angle for that domain. The 180°-switched domain is free from residual stress as the lattice distortion is same for initial and final state of 180° switching, while 109° and 180°-switched domains are associated with additional stress.

Therefore, the domains which showed switching at 5 V can be assigned to either 71° or 109°-type of ferroelectric domain as it requires lesser electrical energy to switch. Whereas those domains that undergo switching at 10 V are 180°-type of ferroelectric domains as they require relatively more electrical energy to switch.

3.1.2 Piezoresponse force spectroscopy. Having observed the switching of domains, we have carried out piezoresponse

force spectroscopy to obtain phase and mag loops in the sample using a continuously varying dc voltage between −10 to +10 V in steps of 0.1 V. Fig. 3 shows the phase and mag loop of pristine BFO ceramic sample in the applied voltage range from −6 to +10 V in forward and backward sweep. In the case of both positive and negative sweep, the piezoresponse is found to increase with increasing applied voltage. We were able to acquire almost symmetrical ferroelectric mag loop (*i.e.* close to perfect butterfly loop) and corresponding symmetrical phase loop. In general, the piezoresponse in a material is due to the sum total of piezoresponses from the spontaneous polarization and the induced polarization through applied voltage. The clear hysteresis behavior observed in phase and mag loop signify that the obtained piezoresponse is because of the ferroelectric behavior. Therefore the symmetrical mag and phase loops demonstrate the ferroelectric behavior of the pristine BiFeO₃ sample.

3.1.2.1 Calculation of piezoelectric coefficient (d₃₃). The piezoelectric coefficient of a material is a measure of response to applied electric field. Here, the longitudinal piezoelectric response is denoted as 'd_{33}', where both electric field and piezoelectric response are in z-direction. The d_{33} value has been calculated by using the piezoresponse force spectroscopy corresponding to $V_{dc} = 0$ V. In a typical PFM, the modulation voltage V_{ac}, which is applied between the tip and the ferroelectric material, leads to a vertical displacement of the tip. Since the tip is in mechanical contact with the sample surface, it precisely follows the piezo force from the sample surface. In the present study, the applied voltage on the microcrystals generates deformation *i.e.*, elongation or contraction of the microcrystal. The piezoelectric coefficient d_{33} has been calculated by using the formula:[50]

$$d_{33} = \Delta S_z / E_z \tag{1}$$

where $E_z = V_{ac}/z$ and $\Delta S_z = \Delta z/z$ is the change of strain along the z-direction. Using the values of E_z and ΔS_z in eqn (1), d_{33} can be written as

$$d_{33} = \Delta S_z / E_z \tag{2}$$

In PFM measurements, the magnitude of the tip vibration measured by the lock-in amplifier technique gives information on the piezoelectric strain. Therefore, the piezoelectric coefficient, d_{33}, can be determined by using the formula as described

Table 1 Comparison of the reported d_{33} value of BiFeO₃ with the present work

Material	Piezoelectric Co-efficient
BFO nanowire	22.21 pm V⁻¹ (max)[51]
BFO thin film	46 pm V⁻¹ for 150 nm film to 8 pm V⁻¹ for 6 nm film[52]
	60 pm V⁻¹ for ≥ 100 nm film[53]
	17 pm V⁻¹ (ref. 54)
BFO polycrystalline ceramics	50–60 pm V⁻¹ (ref. 5)
BFO polycrystalline ceramics	70–80 pm V⁻¹ (present work)

© 2022 The Author(s). Published by the Royal Society of Chemistry

in eqn (2). The value of d_{33} determined over a number of polar domains was found to be 70–80 pm V^{-1}. In Table 1, we have listed the reported d_{33} values of BiFeO$_3$ in various forms of sample and compared with the value obtained from the present study. The obtained d_{33} value is close to the reported value for polycrystalline BiFeO$_3$ sample.[5]

Fig. 4 Topography, mag and phase images of BBFO at a few selected dc voltages. The yellow and white dotted loops are the regions of magnetic domains which show noticeable changes with applied dc voltage.

Further, we have analyzed the ferroelectric behavior of the doped samples through PFM measurements to understand the doping effect on ferroelectric behavior.

3.2 BiFeO$_3$:Ba^{2+} ceramic pellet

3.2.1 PFM studies. Fig. 4 displays the topography, mag and phase images of Ba-doped BiFeO$_3$ sample at a few selected dc voltages in a cyclic order to understand the hysteresis behavior (*i.e.*, at 0, 1, 5, 10, 0, −1, −5, −10 and 0 V). The piezoelectric domains are clearly observed in phase and mag images, which gives evidence of the piezoelectric behavior of the Ba-doped sample. PFM phase images clearly depicted the spatial distribution of piezo domains which are randomly oriented.

Next, we have followed their evolution with respect to applied positive and negative dc voltages to understand the switching behavior in this sample. It is clearly noticed that the observed piezoelectric domains show switching behavior through the reversing of the applied dc voltage. This gives evidence of the ferroelectric behavior in the sample. We have specifically followed a few selected ferroelectric domains (see the domains highlighted with loops) with respect to applied dc voltage. The domains highlighted by yellow colored loops show switching at 5 V and thus these are either 71° or 109°-ferroelectric domains, whereas the domains shown by white loops show switching at 10 V and hence, these domains are 180°-ferroelectric domains.

Ferroelectric nature of the Ba-doped sample is further confirmed through piezoresponse force spectroscopy, discussed below.

3.2.2 Piezoresponse force spectroscopy. Fig. 5 displays the phase and mag loops of the Ba-doped sample obtained in the voltage range from −15 to +15 V. Here again, we were able to acquire nearly symmetric phase and mag loops. It is observed from the phase loop that the piezoelectric domain clearly shows the switching of the polarization by reversing the applied dc voltage and the hysteresis behavior of the domain. The mag loop illustrates the saturation and hysteresis behavior of the domains. Thus, the piezoresponse force spectroscopy clearly
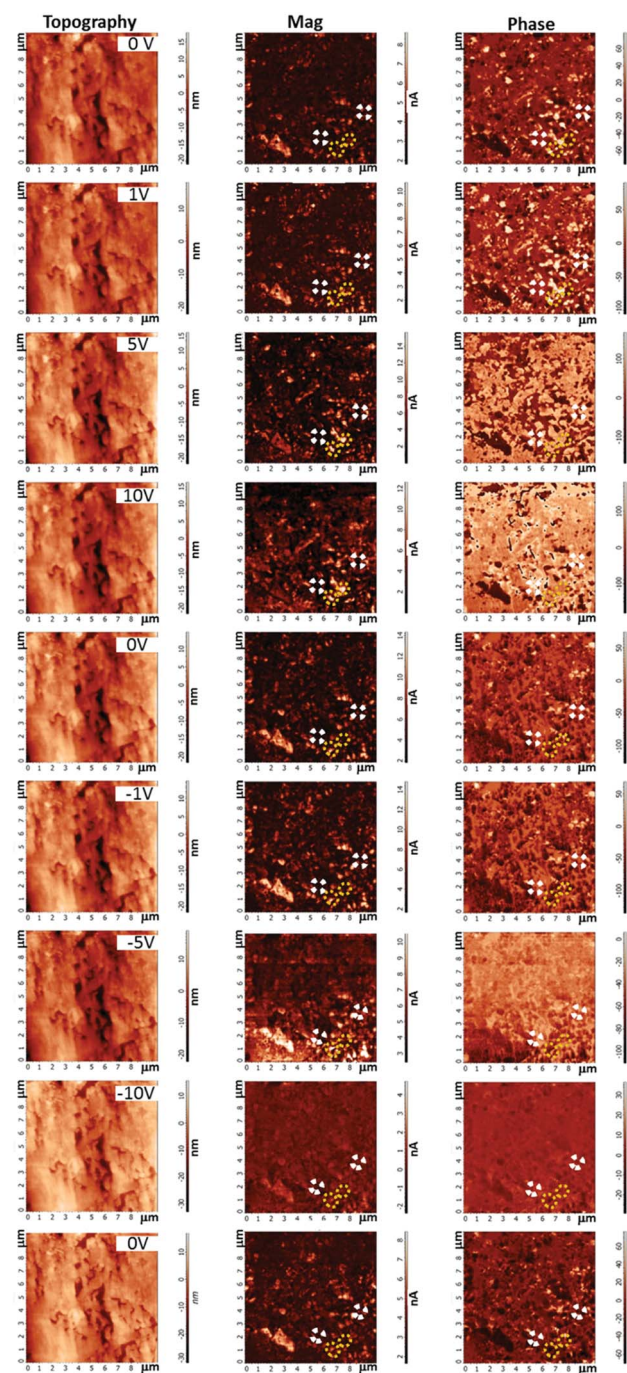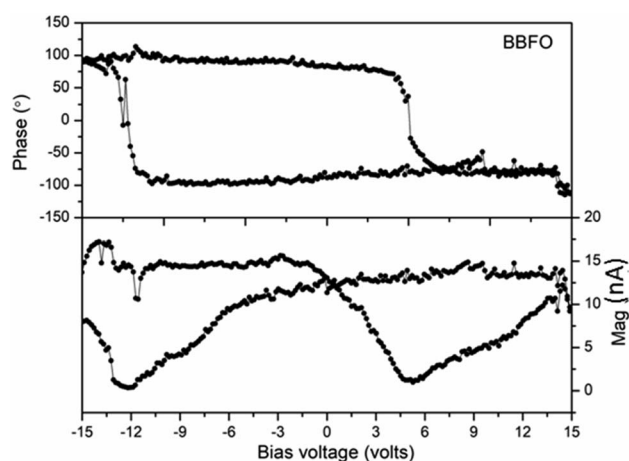

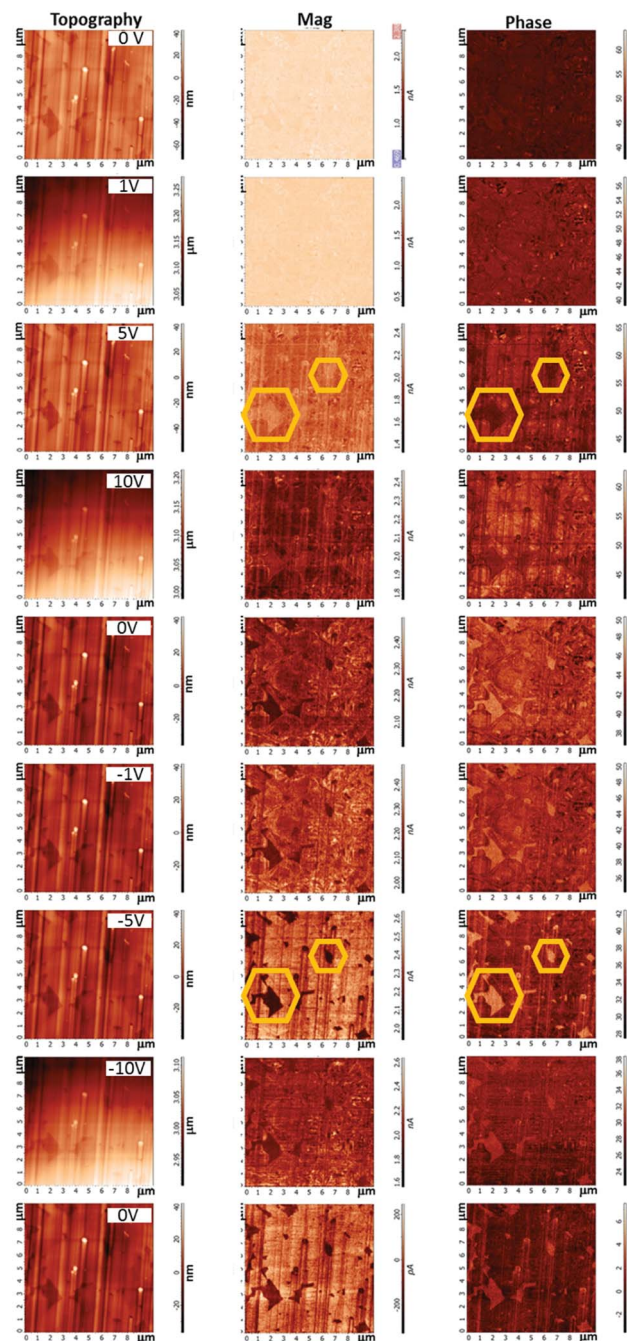**Fig. 5** Phase and mag loops of Ba–doped BFO sample.

Fig. 6 Topography, mag and phase images of BBCFO at few selected dc voltages. Yellow colored loops point to the region of piezo-domains showing polarization switching between +5 V and −5 V.

Fig. 7 Phase and mag loops of Ba–Ca co-doped BFO sample.

Ba^{2+} ion compared to that of Bi^{3+} ion, which helps in preserving the ferroelectric property.

3.3 Ba and Ca co-doped $BiFeO_3$

3.3.1 PFM study. The topography, mag and phase images of co-doped BFO sample are shown in Fig. 6 for various applied dc voltages (0, 1, 5, 10, 0, −1, −5, −10 and 0 V). The acquired PFM images clearly show piezoelectric domains. It is also observed that these domains show evolution with respect to applied dc voltages. If we compare the phase and mag image at a dc voltage of 5 and −5 V, the dark contrast of piezo domains shown by the yellow color hexagon in the phase image at 5 V got changed to bright contrast at −5 V. This shows the polarization switching of piezo domains, which gives evidence of the ferroelectric nature of the sample. The ferroelectric property of the co-doped sample is further investigated through piezoresponse spectroscopy measurements.

3.3.2 Piezoresponse force spectroscopy. Fig. 7 displays the phase and mag loops of the Ba–Ca co-doped sample from PFM measurements. We were able to get switching as well as characteristic hysteresis behavior of the polar domains (see phase loop of Fig. 7). The mag loop shows saturation of the polarization as well as hysteresis behavior of the co-doped sample. Thus, the phase and mag loops give evidence for the existence of ferroelectricity in the co-doped sample.

The piezoelectric coefficient, d_{33}, of the co-doped sample determined by using eqn (2), was found to be in the range of 15–20 pm V^{-1}. This shows that the ferroelectric property is substantially weakened in the co-doped sample. Since we have already seen that Ba doping at Bi^{3+} site does not hamper ferroelectricity much, the main reason for the reduction of the ferroelectric property in the co-doped sample is mainly because of the substitution of 5% Ca^{2+} ion at Bi^{3+} site.

3.4 $BiFeO_3$:Ca^{2+} ceramic pellet

3.4.1 PFM studies. We have also acquired the PFM images of the Ca-doped sample at different applied voltages (0, 5, 10, 0, −5, −10 and 0 V), which are displayed in Fig. 8. The

gives evidence of ferroelectric nature of the Ba-doped $BiFeO_3$ sample.

The piezoelectric coefficient, d_{33}, has been determined by using the formula as described in eqn (2). The d_{33} value determined over a number of polar domains was found to be 70–80 pm V^{-1}, which is similar to the d_{33} value observed in the pristine sample. Although, the lone pair over Bi^{3+} ion is responsible for the ferroelectric property, it is seen that 10% Ba doping at Bi site has not hampered the ferroelectric property of $BiFeO_3$. This may be due to the larger ionic radius of
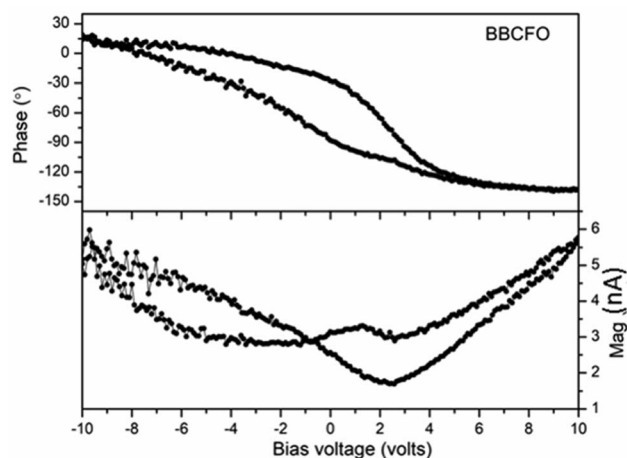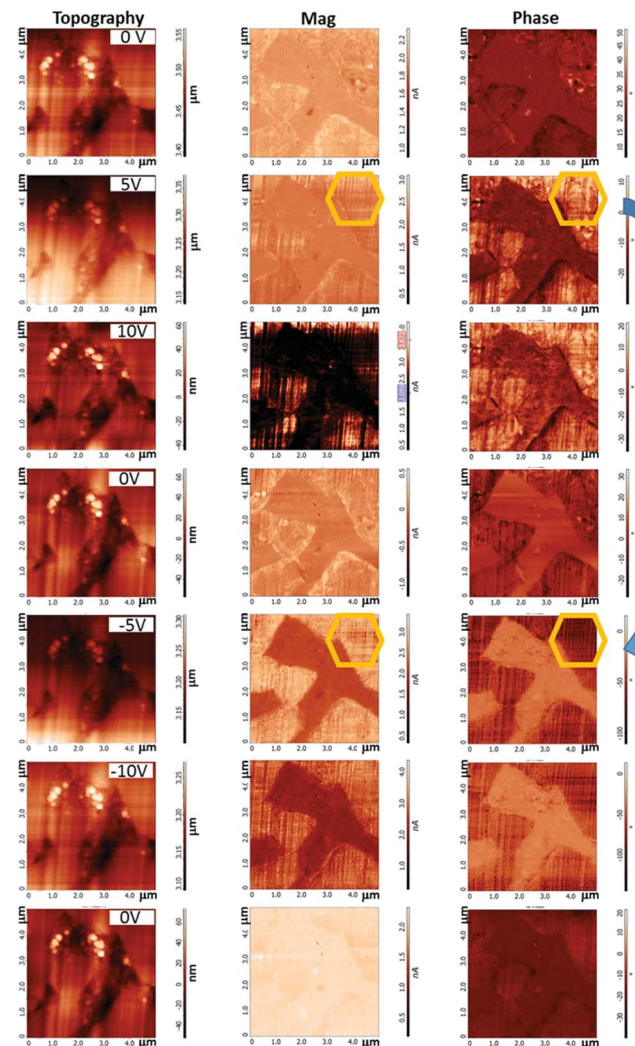
Fig. 8 Topography, mag and phase images of BCFO at a few selected dc voltages. Yellow colored loops point to the region of piezo-domains showing polarization switching between +5 V and −5 V.

Fig. 9 Phase and mag loops of Ca-doped BFO sample.

Thus, the piezoresponse force spectroscopy clearly depicts the ferroelectric property of the Ca-doped sample. The d_{33} value calculated for the Ca-doped sample using eqn (2) is found to be 15–20 pm V^{-1}. Here, the ferroelectric property of the Ca-doped sample is similar to that of co-doped sample, which is significantly reduced on account of Ca doping.

From the PFM measurements, the studied samples are all found to be ferroelectric to different degrees. In particular, Ca^{2+} doping at Bi^{3+} site of BiFeO$_3$ significantly reduced its ferroelectric property, as a result of the simultaneous reduction of sample density and grain size.[44] However Ba^{2+} doping doesn't alter the ferroelectric property, which is due to the larger ionic radius of Ba^{2+} ion compared to that of Bi^{3+}. It should be noted here that all the investigated samples were sintered under same heat treatment conditions and for the same duration.

3.5 MFM studies

The magnetic properties of both the pristine and the doped samples have been investigated through magnetic force

piezoelectric domains are observed both in the phase and mag images. These domains are found to evolve with applied dc voltage. For switching behavior, we have compared phase and mag images of the sample at +5 and −5 V. The contrast of the region shown by the yellow color hexagon (Fig. 8) gets changed from 5 to − 5 V, *i.e.*, from bright to dark. This shows the switching behavior of the polarization with voltage, which gives evidence of the ferroelectric property of the Ca-doped sample. Further, we have investigated the ferroelectric property of the Ca-doped sample through piezoresponse force spectroscopy.

3.4.2 Piezoresponse force spectroscopy. Fig. 9 displays the phase and mag loops through PFM measurements. It is noticed that the piezoelectric domain shows switching behavior with bias voltage and characteristic hysteresis property (see phase loop of Fig. 9). On the other hand, the mag loop is slightly distorted, which could be due to the different orientations of the ferroelectric domains. However, the mag loop shows hysteresis and saturation behavior of the electric polarization.
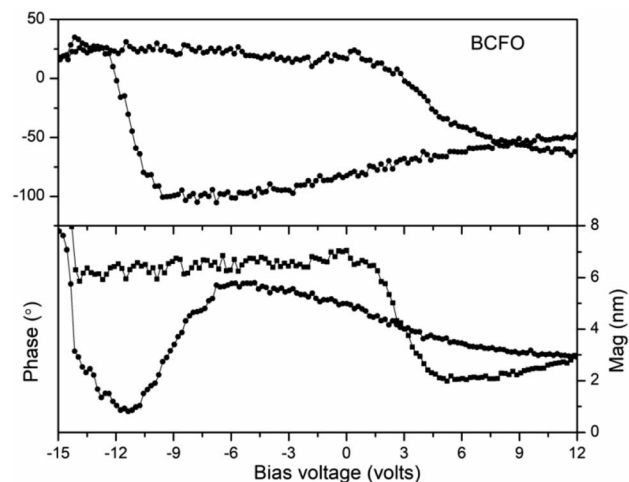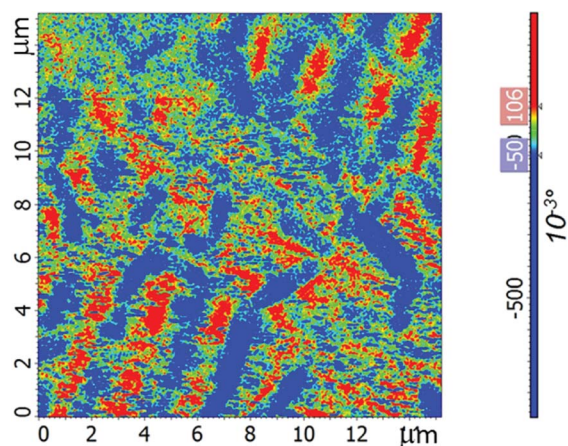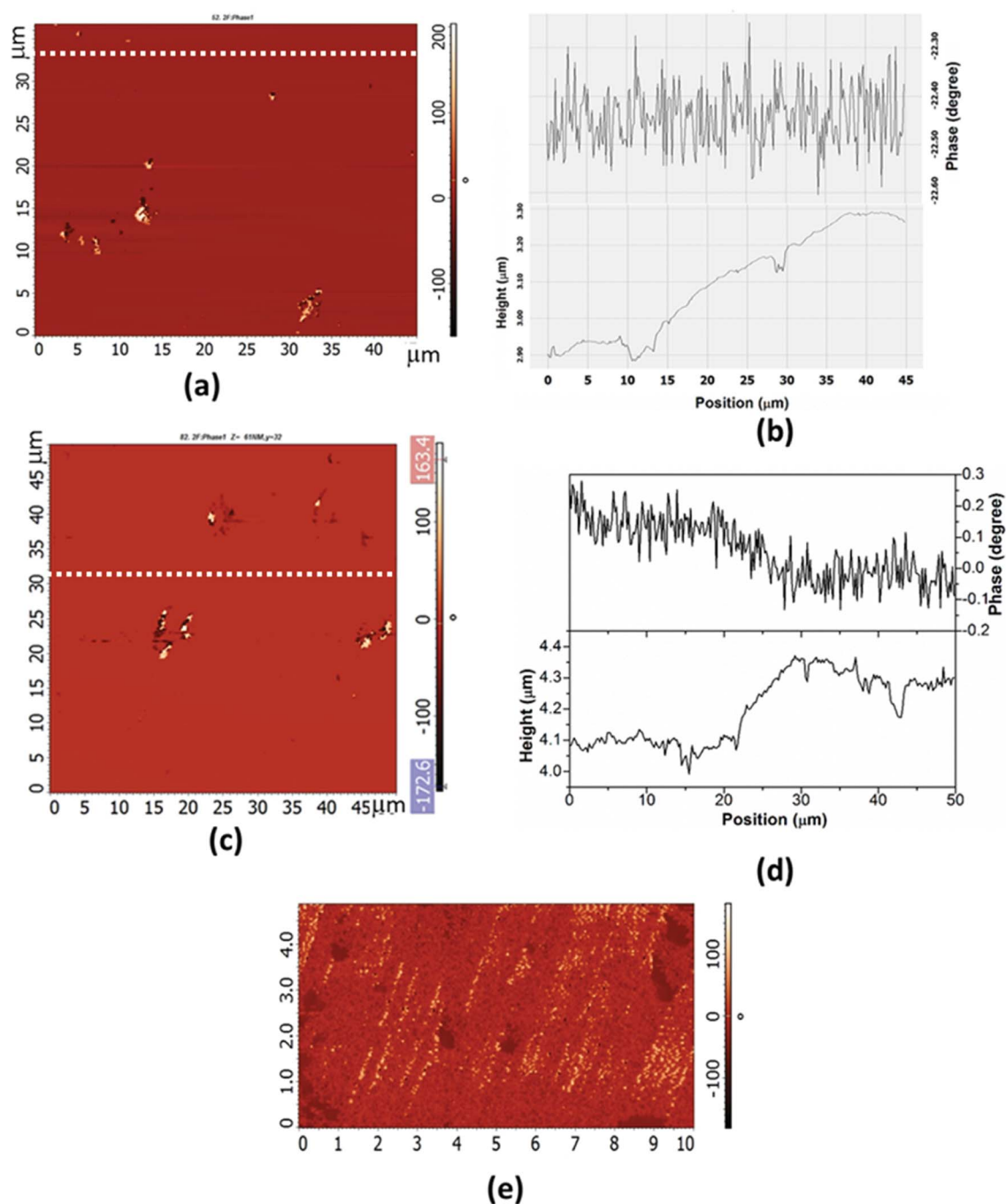

Fig. 10 MFM image a commercial hard disk.

Fig. 11 (a) MFM image and (b) the corresponding line profile of phase and height BFO sample at $y = 35$ μm. (c) MFM image and (d) the corresponding line profile of phase and height BCFO sample at $y = 32$ μm. (e) Expanded region of Fig. 11c showing bright and dark fringes.

microscopy (MFM) measurements. First we have investigated the magnetic behavior of a hard disk through MFM studies and then compared with the magnetic properties of the studied samples. In the MFM phase image of the hard disk (Fig. 10), the magnetic domains, which get magnetized in perpendicularly upward and downward directions, are shown by red and blue colored fringes, respectively, while the magnetic domains which get magnetized along the plane of the hard disk, are shown in green color.

We were able to acquire MFM images of the pristine BFO sample and the 10% Ca-doped sample, which are displayed in Fig. 11a and c, respectively. From the phase image of the pristine sample, we were able to get distinct magnetic domains. From the line profile of the corresponding phase image, the maximum magnitude of the phase deflection is found to be ~0.1°, which gives clear indication of the existence of magnetic domains in the pristine sample. Thus, these MFM data point towards a weak magnetic behavior of the sample. On the other

hand, we have clearly noticed bright and dark fringes in the phase image of BCFO sample shown in Fig. 11e. The dark and bright fringes are represented by the magnetic domains magnetized along upward and downward direction of the sample surface. Moreover, the line profile of the corresponding phase image also show clear evidence of the magnetic domains, as the magnitude of the phase deflection of BCFO is $\sim 0.2°$. These observations point to an enhanced magnetism in BCFO sample. This also correlates well with the observed suppression of SWEs in BCFO sample from the infrared measurements indicating improvement in the magnetic property on account of a significant increase in single ion anisotropy.[37]

4 Conclusion

Piezoelectric and magnetic force microscopy studies have been carried out on both pristine and doped BiFeO$_3$ samples. From the PFM measurements, the distributions of piezoelectric domains are observed in all the studied samples. Moreover, the phase and mag loops of the studied samples obtained from piezoresponse force spectroscopy show switching, saturation and hysteresis behavior. The d_{33} value is calculated from mag loop which is found to be 70–80 pm/V for pristine BiFeO$_3$. We have found that the d_{33} values decrease noticeably from the pristine BiFeO$_3$ case to the Ca-doped case. Concomitantly, the MFM studies on these samples show improved magnetic property for the Ca-doped BiFeO$_3$ as compared to the pristine sample. These results are in complete agreement with our infrared results, where a suppression of the SWE modes leading to enhanced magnetism in Ca-doped BiFeO$_3$ was observed.

Conflicts of interest

There are no conflicts of interest to declare.

Acknowledgements

References

1 B. Ramachandran and M. S. R. Rao, Low temperature magnetocaloric effect in polycrystalline BiFeO$_3$ ceramics, *Appl. Phys. Lett.*, 2009, **95**, 142505.

2 J.-G. Park, M. D. Le, J. Jeong and S. Lee, Structure and spin dynamics of multiferroic BiFeO$_3$, *J. Phys.: Condens. Matter.*, 2014, **26**, 433202.

3 P. Ravindran, R. Vidya, A. Kjekshus, H. Fjellvåg and O. Eriksson, Theoretical investigation of magnetoelectric behavior in BiFeO$_3$, *Phys. Rev. B: Condens. Matter Mater. Phys.*, 2006, **74**, 224412.

4 J. Neaton, C. Ederer, U. Waghmare, N. Spaldin and K. Rabe, First-principles study of spontaneous polarization in multiferroic BiFeO$_3$, *Phys. Rev. B: Condens. Matter Mater. Phys.*, 2005, **71**, 014113.

5 V. Shvartsman, W. Kleemann, R. Haumont and J. Kreisel, Large bulk polarization and regular domain structure in ceramic BiFeO$_3$, *Appl. Phys. Lett.*, 2007, **90**, 172115.

6 R. Zeches, M. Rossell, J. Zhang, A. Hatt, Q. He, C.-H. Yang, A. Kumar, C. Wang, A. Melville and C. Adamo, A strain-driven morphotropic phase boundary in BiFeO$_3$, *Science*, 2009, **326**, 977.

7 A. J. Hatt, N. A. Spaldin and C. Ederer, Strain-induced isosymmetric phase transition in BiFeO$_3$, *Phys. Rev. B: Condens. Matter Mater. Phys.*, 2010, **81**, 054109.

8 C. Xu, B. Xu, B. Dupé and L. Bellaiche, Magnetic interactions in BiFeO$_3$: A first-principles study, *Phys. Rev. B: Condens. Matter Mater. Phys.*, 2019, **99**, 104420.

9 I. Sosnowska and A. K. Zvezdin, Origin of the long period magnetic ordering in BiFeO$_3$, *J. Magn. Magn. Mater.*, 1995, **140–144**, 167–168.

10 J. Gebhardt and A. M. Rappe, Doping of BiFeO$_3$: A comprehensive study on substitutional doping, *Phys. Rev. B: Condens. Matter Mater. Phys.*, 2018, **98**, 125202.

11 S. Gupta, M. Pal, M. Tomar, R. Guo, A. Bhalla and V. Gupta, Ferroelectric and magnetic domain mapping of magneto-dielectric Ce doped BiFeO$_3$ thin films, *J. Alloys Compd.*, 2021, **882**, 160698.

12 D. V. Karpinsky, M. V. Silibin, A. V. Trukhanov, A. L. Zhaludkevich, T. Maniecki, W. Maniukiewicz, V. Sikolenko, J. A. Paixão and V. A. Khomchenko, A correlation between crystal structure and magnetic properties in co-doped BiFeO$_3$ ceramics, *J. Phys. Chem. Solids*, 2019, **126**, 164.

13 F. S. Jesús, A. M. Bolarín-Miro, C. A. Cortes-Escobedo, A. Barba-Pingarron and F. Pedro-García, Enhanced ferromagnetic and electric properties of multiferroic BiFeO$_3$ by doping with Ca, *J. Alloys Compd.*, 2020, **824**, 153944.

14 T. Wang, S.-H. Song, Q. Ma, M.-L. Tan and J.-J. Chen, Highly improved multiferroic properties of Sm and Nb co-doped BiFeO$_3$ ceramics prepared by spark plasma sintering combined with sol–gel powders, *J. Alloys Compd.*, 2019, **795**, 60.

15 I. Makoed, V. Prigodich, K. Yanushkevich, A. Zhivulko, V. Zhivulko, A. Galias, O. Demidenko and D. Krivchenya, Effect of Co-Doping on Magnetic Properties of Bismuth Ferrite, *Acta Phys. Pol., A*, 2020, **137**, 985.

16 A. Molaka, D. K. Mahato and A. Z. Szeremet, Synthesis and characterization of electrical features of bismuth manganite and bismuth ferrite: effects of doping in cationic and anionic sublattice: Materials for applications, *Prog. in Cryst. Growth and Charact.of Mats.*, 2018, vol. 64, p. 1.

17 H. Yamamoto, T. Kihara, K. Oka, M. Tokunaga, K. Mibu and M. Azuma, Spin Structure Change in Co-Substituted BiFeO$_3$, *J. Phys. Soc. Jpn.*, 2016, **85**, 064704.

18 Z. V. Gareeva, K. A. Zvezdin, A. P. Pyatakov and A. K. Zvezdin, Novel type of spin cycloid in epitaxial bismuth ferrite films, *J. Magn. Magn. Mater.*, 2019, **469**, 593.

19 S. R. Burns, O. Paull, J. Juraszek, V. Nagarajan and D. Sando, The Experimentalist's Guide to the Cycloid, or Noncollinear

Antiferromagnetism in Epitaxial $BiFeO_3$, *Adv. Mater.*, 2020, **32**, 2003711 and references therein.

20 F. Bai, J. Wang, M. Wuttig, J. Li, N. Wang, A. P. Pyatakov, A. Zvezdin, L. Cross and D. Viehland, Destruction of spin cycloid in (111) c-oriented $BiFeO_3$ thin films by epitiaxial constraint: enhanced polarization and release of latent magnetization, *Appl. Phys. Lett.*, 2005, **86**, 032511.

21 G. A. Gomez-Iriarte, C. Labre, L. A. S. de Oliveira and J. P. Sinnecker, Pure phase $BiFeO_3$ thin films sputtered over Si: A new route towards high magnetization, *J. Magn. Magn. Mater.*, 2018, **460**, 83.

22 S. Huang, F. Hong, Z. Xia, F. Yang, X. Zhang, G. Xiao, Y. Song, D. Jiang, H. Deng, Z. Ouyang, J. Wang, Z. Tian, J. Han, L. Yao, A. Forget, D. Colson and Z. Cheng, Multiferroic behavior from synergetic response of multiple ordering parameters in $BiFeO_3$ single crystal under high magnetic field up to 50 Tesla, *J. Appl. Phys.*, 2020, **127**, 044101.

23 S. Kawachi, S. Miyahara, T. Ito, A. Miyake, N. Furukawa, J. Yamaura and M. Tokunaga, Direct coupling of ferromagnetic moment and ferroelectric polarization in $BiFeO_3$, *Phys. Rev. B*, 2019, **100**, 140412–1.

24 M. Tokunaga, M. Akaki, T. Ito, S. Miyahara, A. Miyake, H. Kuwahara and N. Furukawa, Magnetic control of transverse electric polarization in $BiFeO_3$, *Nat. Commun.*, 2015, **6**, 5878.

25 U. Nagel, R. S. Fishman, T. Katuwal, H. Engelkamp, D. Talbayev, H. Taek Yi, S.-W. Cheong and T. Room, Terahertz Spectroscopy of Spin Waves in Multiferroic $BiFeO_3$ in High Magnetic Fields, *Phys. Rev. Lett.*, 2013, **110**, 257201.

26 R. S. Fishman, Field dependence of the spin state and spectroscopic modes of multiferroic $BiFeO_3$, *Phys. Rev. B: Condens. Matter Mater. Phys.*, 2013, **87**, 224419.

27 M. Tokunaga, M. Azuma and Y. Shimakawa, High-field study of multiferroic $BiFeO_3$, *J. Phys.: Conf. Ser.*, 2010, **200**, 012206.

28 J. Buhot, C. Toulouse, Y. Gallais, A. Sacuto, R. de Sousa, D. Wang, L. Bellaiche, M. Bibes, A. Barthélémy, A. Forget, D. Colson, M. Cazayous and M.-A. Measson, Driving spin excitations by hydrostatic pressure in $BiFeO_3$, *Phys. Rev. Lett.*, 2015, **115**, 267204.

29 D. P. Kozlenko, A. A. Belik, A. V. Belushkin, E. V. Lukin, W. G. Marshall, B. N. Savenko and E. Takayama-Muromachi, Antipolar phase in multiferroic $BiFeO_3$ at high pressure, *Phys. Rev. B: Condens. Matter Mater. Phys.*, 2011, **84**, 094108.

30 R. Haumont, P. Bouvier, A. Pashkin, K. Rabia, S. Frank, B. Dkhil, W. A. Crichton, C. A. Kuntscher and J. Kreisel, Effect of high pressure on multiferroic $BiFeO_3$, *Phys. Rev. B: Condens. Matter Mater. Phys.*, 2009, **79**, 184110.

31 E. Ramos, A. Cardona-Rodriguez, D. Carranza-Celis, R. Gonzalez-Hernandez, D. Muraca and J. G. Ramírez, Strain-controlled ferromagnetism in $BiFeO_3$ nanoparticles, *J. Phys.: Condens. Matter*, 2020, **32**, 185703.

32 I. Aupiais, P. Hemme, M. Allen, A. M. Scida, X. Lu, C. Ricolleau, Y. Gallais, A. Sacuto, S. S. Wong, R. de Sousa and M. Cazayous, Impact of the surface phase transition on magnon and phonon excitations in $BiFeO_3$ nanoparticles, *Appl. Phys. Lett.*, 2020, **116**, 172903.

33 W. Li, F. Wang, G. Fu, Z. Ren and G. Han, Ferroelectric Polarization Induced Selective Growth of $BiFeO_3$ Nanocrystals with a Remarkable Ferromagnetism, *Eur. J. Inorg. Chem.*, 2019, 1945.

34 N. A. Lomanova, V. V. Panchuk, V. G. Semenov, I. V. Pleshakov, M. P. Volkov and V. V. Gusarov, Bismuth orthoferrite nanocrystals: magnetic characteristics and size effects, *Ferroelectrics*, 2020, **569**, 240.

35 J. Bertinshaw, R. Maran, S. J. Callori, V. Ramesh, J. Cheung, S. A. Danilkin, W. T. Lee, S. Hu, J. Seidel and N. Valanoor, Direct evidence for the spin cycloid in strained nanoscale bismuth ferrite thin films, *Nat. Commun.*, 2016, **7**, 12664.

36 J. Landers, S. Salamon, M. Escobar Castillo, D. Lupascu and H. Wende, Mossbauer study of temperature-dependent cycloidal ordering in $BiFeO_3$ nanoparticles, *Nano Lett.*, 2014, **14**, 6061.

37 B. K. Das, T. N. Sairam, R. Balakrishnan and M. R. Rao, Chemical pressure induced near-complete suppression of spin-wave excitations in $Bi_{0.9}A_{0.1}FeO_{2.95}$ (A= Ba, Ca), *J. Phys. D: Appl. Phys.*, 2020, **53**, 495302.

38 B. Ramachandran and M. R. Rao, Low temperature magnetocaloric effect in polycrystalline $BiFeO_3$ ceramics, *Appl. Phys. Lett.*, 2009, **95**, 142505.

39 B. K. Das, B. Ramachandran, A. Dixit, M. R. Rao, R. Naik, A. Sathyanarayana, T. N. Sairam and G. Amarendra, Emergence of two-magnon modes below spin-reorientation transition and phonon-magnon coupling in bulk $BiFeO_3$: An infrared spectroscopic study, *J. Alloys Compd.*, 2020, 154754.

40 J. Jeong, M. D. Le, P. Bourges, S. Petit, S. Furukawa, S.-A. Kim, S. Lee, S. W. Cheong and J.-G. Park, Temperature-Dependent Interplay of Dzyaloshinskii-Moriya Interaction and Single-Ion Anisotropy in Multiferroic $BiFeO_3$, *Phys. Rev. Lett.*, 2014, **113**, 107202.

41 B. K. Das, T. N. Sairam, R. Balakrishnan and M. S. R. Rao, Single-ion anisotrpy driven splitting of spin wave resonances in $BiFeO_3$ at low temperature, *J. Phys.: Condens. Matter*, 2020, **32**, 405701.

42 B. Ramachandran, A. Dixit, R. Naik, G. Lawes and M. Ramachandra Rao, Dielectric relaxation and magneto-dielectric effect in polycrystalline $Bi_{0.9}Ca_{0.1}FeO_{2.95}$, *Appl. Phys. Lett.*, 2012, **100**, 252902.

43 R. Balakrishnan, A. Dixit, R. Naik and M. S. R. Rao, Enhancement in electrical and magnetodielectric properties of Ca-and Ba-doped $BiFeO_3$ polycrystalline ceramics, *J. Am. Ceram. Soc.*, 2018, **101**, 782–788.

44 B. Ramachandran, A. Dixit, R. Naik, G. Lawes and M. Ramachandra Rao, Weak ferromagnetic ordering in Ca doped polycrystalline $BiFeO_3$, *J. Appl. Phys.*, 2012, **111**, 023910.

45 S. V. Kalinin and D. A. Bonnell, Imaging mechanism of piezoresponse force microscopy of ferroelectric surfaces, *Phys. Rev. B: Condens. Matter Mater. Phys.*, 2002, **65**, 124508.

46 R. K. Vasudevan, S. Jesse, Y. Kim, A. Kumar and S. V. Kalinin, Spectroscopic imaging in piezoresponse force microscopy:

New opportunities for studying polarization dynamics in ferroelectrics and multiferroics, *MRS Commun.*, 2012, **2**, 61–73.

47 O. Kazakova, R. Puttock, C. Barton, H. Corte-León, M. Jaafar, V. Neu and A. Asenjo, Frontiers of magnetic force microscopy, *J. Appl. Phys.*, 2019, **125**, 060901.

48 Y. Jin, X. Lu, J. Zhang, Y. Kan, H. Bo, F. Huang, T. Xu, Y. Du, S. Xiao and J. Zhu, Studying the Polarization Switching in Polycrystalline BiFeO$_3$ Films by 2D Piezoresponse Force Microscopy, *Sci. Rep.*, 2015, **5**, 12237.

49 S. Baek and C. Eom, Reliable polarization switching of BiFeO$_3$, *Philos. Trans. R. Soc., A*, 2012, **370**, 4872–4889.

50 A. Gruverman and S. V. Kalinin, Piezoresponse force microscopy and recent advances in nanoscale studies of ferroelectrics, *J. Mater. Sci.*, 2006, **41**, 107–116.

51 S. Wu, J. Zhang, X. Liu, S. Lv, R. Gao, W. Cai, F. Wang and C. Fu, Micro-area ferroelectric, piezoelectric and conductive properties of single BiFeO$_3$ nanowire by scanning probe microscopy, *Nanomaterials*, 2019, **9**, 190.

52 J. Zhao, H. Lu, J. Sun and B. Shen, Thickness dependence of piezoelectric property of ultrathin BiFeO$_3$ films, *Phys. B*, 2012, **407**, 2258–2261.

53 Y. Chu, T. Zhao, M. Cruz, Q. Zhan, P. Yang, L. Martin, M. Huijben, C.-H. Yang, F. Zavaliche and H. Zheng, Ferroelectric size effects in multiferroic BiFeO$_3$ thin films, *Appl. Phys. Lett.*, 2007, **90**, 252906.

54 J. M. Vila-Fungueiriño, A. Gómez, J. Antoja-Lleonart, J. Gázquez, C. Magén, B. Noheda and A. Carretero-Genevrier, Direct and converse piezoelectric responses at the nanoscale from epitaxial BiFeO$_3$ thin films grown by polymer assisted deposition, *Nanoscale*, 2018, **10**, 20155–20161.